2007 IEEE International Conference on
Robotics and Automation
Roma, Italy, 10-14 April 2007

Rapidly Prototyped Orthotweezers for Automated Microassembly

Aaron M. Hoover
Dept. of Mechanical Engineering
University of California, Berkeley
ahoover@eecs.berkeley.edu

Ronald S. Fearing
Dept. of Electrical Engineering and Computer Science
University of California, Berkeley
ronf@eecs.berkeley.edu

***Abstract*— We describe the design, fabrication, and testing of an ultra-low cost Orthotweezers system for microassembly. By utilizing rapid prototyping technology, compliant mechanisms, and commodity-grade actuators and sensors, we significantly reduce the complexity and cost of the previous Orthotweezers system without sacrificing functionality. With a force resolution of 0.7mN and a worst case mean positioning repeatability of 23μm, the system is capable of dextrously manipulating rectangular parts with dimensions 200μm x 200μm x 100μm. Such blocks can then be temporarily attached to thin, delicate, or oddly shaped parts to enable handling and ultimately assembly of micromechanical structures. Strategies for using compliance to compensate for uncertainty introduced by less expensive fabrication methods, actuators, and sensors are also discussed.**

I. INTRODUCTION

Automated robotic microassembly has been an increasing area of research interest driven by a need to assemble ever-smaller components, be they MEMS structures composing hybrid devices, micro-sensors such as strain gages for force and displacement sensing, or microactuators like piezoelectric stacks or beams for small robotic structures. Given that many of these components are produced using planar fabrication processes, the production of 3D structures requires some post-fabrication microassembly step(s).

To that end, much work has already been done in the microassembly/micromanipulation domain using many different approaches. Shen [12] has developed a platform for human/robot tele-microassembly of MEMS devices that allows for cooperative assembly over networks. Pawashe [11] demonstrated an autonomous, vision-based approach to manipulating polystyrene and silica microspheres using an atomic force microscope. Anis recently demonstrated a vision-based method for measuring micrograpping forces in order to identify successful object grasps [2]. Neild et al. have pursued micromanipulation in a fluid [10], showing that microparticles can be precisely aligned using force fields generated by ultrasonic excitation of the fluid, and those particles can then be manipulated using a microgripper. Wierzbicki et al. [18] have even developed an electrostatically actuated microgripper suitable for manipulating blood vessels, while Horie et al. [6] have demonstrated a molded compliant pantograph mechanism for handling surface mount components.

Our broad aim is to demonstrate an entire ultra-low cost microassembly cell for rapidly prototyping micromechatronic and millirobotic structures that can itself be rapidly prototyped/assembled for less that $1000. Guided by this broad aim and using the design goals previously outlined in [5], the system should be comprised of commodity hardware wherever possible, and custom parts should be manufacturable in a way that allows the system to be copied and redistributed. In keeping with this approach, we aim to use only open source, free software, and to make any code we develop freely available as well.

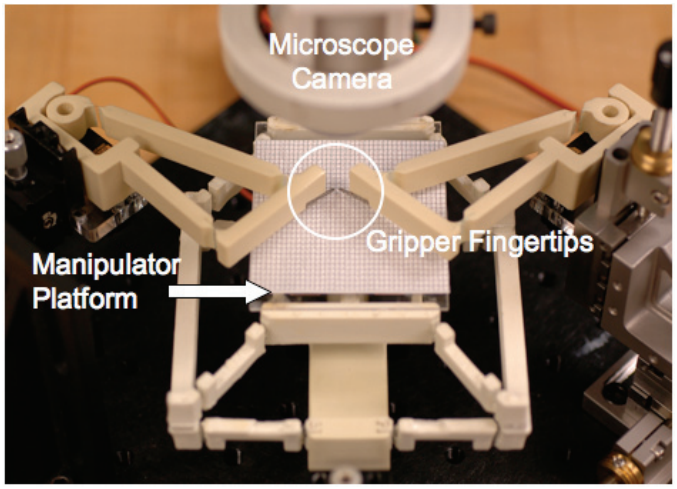

Fig. 1. The Low Cost Orthotweezers system including, 2 axis parallel planar manipulator, Orthotweezers, and low-cost camera for vision-based measurement and feedback

In contrast, the current Orthotweezers system [13] as a platform for prototyping micromechanical structures or millirobotic structures, however, has some major disadvantages. The design relies on expensive ultra-high precision stepper motors and stages for positioning, piezoelectric bending actuators for actuation (and the accompanying high voltage amplifiers needed to drive them), and delicate and often unreliable (due to thermal drift) strain gage sensors for force sensing and feeback control of grasping. The sum total of the hardware alone (including microscopes and cameras for image and movie capture) brings the cost to approximately $20K. Such system complexity and cost impede the generation of interest in prototyping millirobotic structures.

As a basis for a low-cost system, we begin by presenting a design for a planar parallel manipulator with novel kinematics that is fabricated inexpensively using compliant mechanisms and rapid prototyping processes that include

layered manufacturing and molding with insertion. In previous work [5] we have presented a two axis manipulator based on large numbers of parallel flexures using distributed compliance. The planar manipulator design used in this work represents an improvement over the previous design in terms of compactness and high stiffness in off-axis directions even at large displacements. Horie et al. [6] were some of the first to present a compliant parallel mechanism fabricated from molded polymer for use in micromanipulation tasks. And, similarly, we have chosen a low-cost polymer molding process with compliant, large-displacement polymer hinges. However, by inserting separate polymer film strips (PET) into the mold we fabricate fully 3-D large displacement ($\pm$ 45°) hinges that make use of the crossed strip flexure design [17] while taking advantage of the stiffness, and fast-curing properties of fiber reinforced polyurethane for our rigid members. Also, in contrast to the work in [6], the end effector of the manipulator presented here is used as a two axis positioning stage for our micromanipulation tasks and as such the compliant hinges and the balanced mechanism geometry are designed to achieve high off-axis stiffness and to be actuated using inexpensive rotary actuators such as RC servo motors. In the design of the manipulator kinematic restrictions on actuation, workspace area, and manipulability as well as ease and cost of manufacture are considered.

Next, we present a new design for a compliant gripper in which the gripper arms are oriented orthogonally, called Orthotweezers. The principle of orthogonal gripper tips has been presented previously in [13] and [15], and was shown to be a robust approach to grasping microparts. In the Orthotweezers, a simplified model of which is shown in Fig. 2, complete manipulability of parts is obtained by combining a three axis translational stage with two 1DOF fingers. Parts can be grasped and reoriented using simple fixtures. The latest design revision uses rapid prototyping processes to adapt the Orthotweezers concept to allow the grippers to be actuated with significantly cheaper rotary actuators using position rather than force control. The approach presented here also greatly reduces the overall complexity of the system.

For automated calibration of the manipulator we present a very low cost vision system using inexpensive, commercially available hardware and a simple image processing-based approach with a specially designed calibration pattern that simplifies localization. Using a binary planar position encoding scheme, we enable extraction of absolute position in cartesian task space from a single image. While the vision system currently provides feedback for manual operation of the gripper, it has not yet been integrated to provide automated closed loop feedback for grasping.

Lastly we present experimental results of our first attempts at positioning and manipulation with the system.

II. MANIPULATOR DESIGN AND FABRICATION

A. Parallel Manipulator Design

A parallel mechanism is a kinematic mechanism in which the end effector is connected to the base by two or more

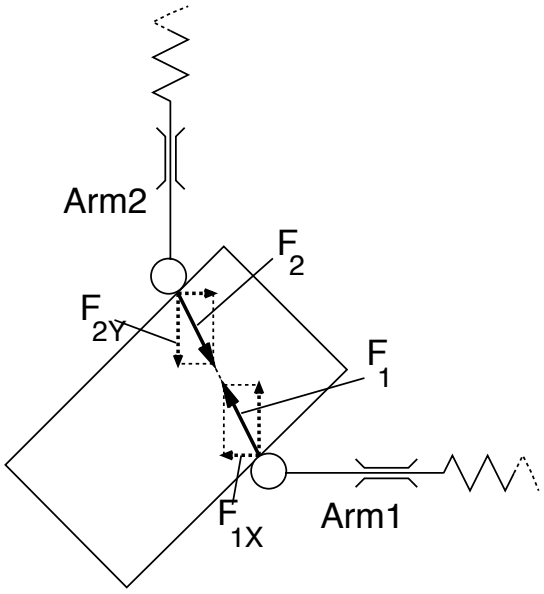

Fig. 2. Rigid body model of orthogonal tweezer tips

kinematic chains. Also occasionally referred to as "closed-chain" mechanisms, the advantages of parallel manipulators are many fold and well known. Compared to their serial counterparts, parallel mechanisms have lower inertia, are compact, provide high stiffness, and are less susceptible to error accumulation. The disadvantages of parallel manipulators are their forward kinematics are generally coupled, nonlinear, and non-trivial (if possible at all) to write in closed form; they generally have smaller workspaces than their serial counterparts, and they are considered less dextrous.

While it is true that a parallel kinematic mechanism like the classic Gough-Stewart platform [14] has complicated forward kinematics, in our case, our need is for only two planar DOFs. This design requirement greatly reduces the space of possible mechanism configurations as well as the kinematic complexity of the candidate manipulators.

The configuration we have chosen is what we call a "planar balanced double four bar" mechanism similar to work presented in [4]. The mechanism consists of an end effector connected to ground through two sets of two serially connected four bar mechanisms. In our final design one four bar linkage is placed in the plane above the other in each of the serial kinematic chains, but for the purpose of simplifying the illustration a kinematic equivalent is depicted in Fig. 3. In the figure, the angles θ_1 and θ_3 are actuated. The outer frame to which the coupler of the second four bar linkage in each chain is attached is the end effector and it is drawn in the plane merely for simplicity in this figure. In practice, the four bars can be attached to the same rigid end effector in such a way that the end effector in no way interferes with the links of either four bar.

1) Manipulator Kinematics: From the figure we see that by choosing the two side links of each four bar to be equal lengths, we prevent rotation of the coupler link. Connecting

the two coupler links at the ends of each kinematic chain creates a balanced structure and provides two translational degrees of freedom from the two rotational inputs. Thus, we observe from the figure that this is a $2\underline{R}RR$ parallel mechanism where the underline indicates the actuated joint.

The relative simplicity of our mechanism allows for the closed form analytical solutions to both the forward (obtaining the end effector pose from the actuator angles) and inverse (obtaining the actuator angles from a prescribed end effector pose) kinematics problems. The forward kinematics can be solved relatively easily, though their closed form solution is ultimately somewhat unwieldy to write out.

To express the kinematic equations more efficiently, we begin by defining quantities, K_1, K_2, α, and β.

$$K_1 = \left(\frac{l_1}{l_2}\right) * (\cos\theta_3 - \cos\theta_1) \tag{1}$$

$$K_2 = \left(\frac{d-a}{l_2} + \frac{l_1}{l_2}\right) * (\sin\theta_3 - \sin\theta_1) \tag{2}$$

$$\alpha = K_2 + \sin\left(\arcsin\left(\frac{\sqrt{K_1^2+K_2^2}}{2}\right) - \arctan\left(\frac{K_1}{K_2}\right)\right) \tag{3}$$

$$\beta = K_1 + \cos\left(\arcsin\left(\frac{\sqrt{K_1^2+K_2^2}}{2}\right) - \arctan\left(\frac{K_1}{K_2}\right)\right) \tag{4}$$

The 2×1 vector, $\mathbf{X}$, represents the position in cartesian space of the end of the upper right link of the upper-most four bar linkage in Fig. 3 and is written in terms of K_1, K_2, α, and β as follows:

$$\mathbf{X} = \begin{pmatrix} \hat{l_1}\sin\theta_1 + \hat{l_2}\sin\left(\arctan\left(\frac{\alpha}{\beta}\right)\right) \\ \hat{l_1}\cos\theta_1 + \hat{l_2}\cos\left(\arctan\left(\frac{\alpha}{\beta}\right)\right) \end{pmatrix} \tag{5}$$

$\hat{l_1}$ and $\hat{l_2}$ are the non-dimensional link lengths that result from dividing l_1 and l_2 each by the quantity $d-a$.

The solution to the inverse kinematics is no more difficult than the forward kinematics, but for our purposes only the forward kinematics are necessary to proceed with our analysis of the manipulator mechanism. Specifically, having a closed form expression for the forward kinematics enables us to visualize the manipulator workspace for different link lengths l_1 and l_2 as well as derive an expression for the Jacobian at any position, $\mathbf{X} = [f_1(\theta_1,\theta_3) \quad f_2(\theta_1,\theta_3)]^T$, defined as:

$$J(\mathbf{\Theta}) = \begin{pmatrix} \frac{\partial f_1}{\partial \theta_1} & \frac{\partial f_1}{\partial \theta_3} \\ \frac{\partial f_2}{\partial \theta_1} & \frac{\partial f_2}{\partial \theta_3} \end{pmatrix} \tag{6}$$

(The actual closed form expression for the Jacobian of the manipulator, however, is long and cumbersome, so it has not been included here). The Jacobian of the forward kinematics represents a map from actuator velocities in the joint or configuration space to velocities of the end effector in the cartesian task space. As such, the Jacobian provides a means for measuring the manipulability of the end effector.

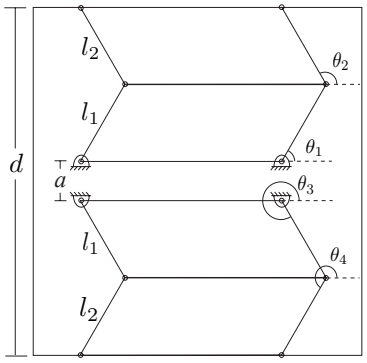

Fig. 3. Kinematically equivalent rigid body model of balanced double four-bar mechanisms

In this case, we define manipulability as the ability of the end effector to change position at a given location [9]. Clearly, the condition number, κ, of the Jacobian provides a measure manipulability as shown in Figs. 4 and 5 :

$$M = \kappa(J(\mathbf{\Theta})) = \frac{\sigma_{max}(J(\mathbf{\Theta}))}{\sigma_{min}(J(\mathbf{\Theta}))} \tag{7}$$

Values of M equal to unity indicate isotropy of the workspace at a given position, and we can further describe a measure of the global uniformity of manipulability using the following measure:

$$U = \frac{M_{min}}{M_{max}} \tag{8}$$

The value of U will always be positive and less than or equal to one and values near unity are desirable, indicating a truly isotropic workspace.

2) Design Parameters: To simplify the exploration of the design space and reduce the number of independent parameters, it is useful to non-dimensionalize the link lengths, l_1 and l_2, by dividing them by the quantity $d-a$. The non-dimensional link lengths are referred to as $\hat{l_1}$ and $\hat{l_2}$. The servo motors that will be used to actuate the manipulator fix the θ_1 and θ_3 ranges to each be less than 120°. So, by careful choice of manipulator geometry, we are able to avoid both type I (loss of a degree of freedom) and type II (gain of a degree of freedom when all actuators are locked) singularities. Design parameters are listed in Table I. A plot of positions in the workspace with their corresponding manipulability ellipsoids for the design parameters listed in Table I is shown in Fig. 5. In this figure the positions are generated by stepping in regular increments in both directions in the Θ space, demonstrating the coupled non-linearity of the forward kinematics. Fig. 4 shows the manipulability of the mechanism plotted as a function of position in the cartesian task space with M_{max} = 3.8 and M_{min} = 1.5.

3) Flexure Joint Design: Because they are inexpensive to produce, exhibit no backlash when designed properly, require no lubrication, are not subject to wear, and can be monolithically fabricated, flexure joints were chosen over

TABLE I

DESIGN PARAMETERS FOR PLANAR BALANCED FOUR BAR PARALLEL MANIPULATOR

Parameter	Value
$\hat{l_1}$	1.17
$\hat{l_2}$	1.17
$(\theta_{1min}, \theta_{1max})$	(45°, 135°)
$(\theta_{3min}, \theta_{3max})$	(-135°, -45°)

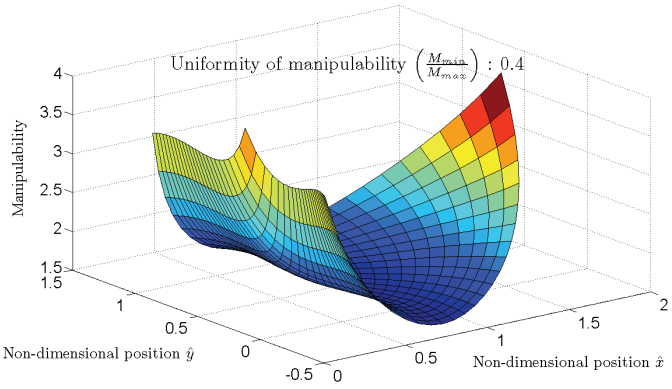

Fig. 4. Manipulability as a function of cartesian task space position

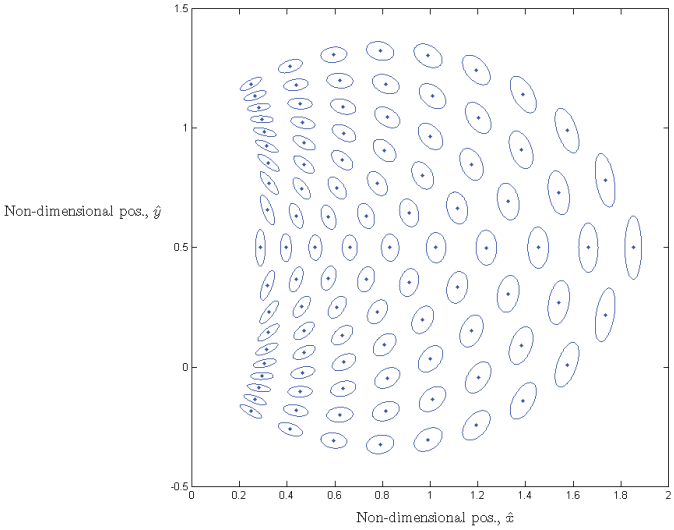

Fig. 5. Scaled manipulability ellipsoids shown at 100 points in the task space

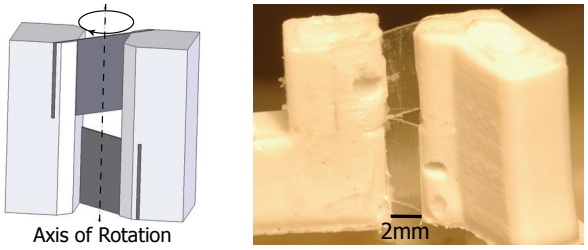

(a) CAD model of crossed strip flexure hinge

(b) Crossed strip flexure hinge (w/ PET flexures) integrated into manipulator

Fig. 6.

conventional pin joints to provide the rotational degree of freedom at each of the joints in the mechanism. In particular, because the joints are subject to large rotational displacements (>20°), we have chosen to approximate the pin joints with the crossed strip flexure [17], a model of which is shown in Fig. 6(a). The angled orientation of the individual flexures in the cross flexure allows them to be longer, increasing their bending radius which produces lower strains than the flat single flexure for the same angular displacement [7] [16]. The cross flexure also exhibits higher off-axis stiffness than the flat flexure alternative. However, compared to other designs of revolute flexure mechanisms, the cross flexure is still relatively simple to manufacture.

B. Fabrication

Though we have so far modeled the manipulator as a set of ideal rigid links connecting a ground to an end effector, the actual manipulator is fabricated nearly monolithically as a compliant mechanism using a combination of rapid prototyping techniques.

First, it should be noted that the actual manipulator places the second four bar linkage in each of the two kinematic chains in a plane above the first and folds the links back in the direction of ground. Kinematics of this configuration are equivalent to those in Fig. 3; this is done simply to make the manipulator more spatially compact. The end effector connects the two coupler links of the second four bar linkage in each chain, and the surface of the end effector platform translates in yet a third plane parallel to, but above the plane of the second four bar linkage.

The fabrication process for the manipulator is nearly identical to the process previously described in [5], and bears some resemblance to shape deposition manufacturing (SDM) [8] insofar as functional compliant members are molded individually first, and later inserted into a larger mold to form the whole structure.

The first step in the mechanism fabrication is the creation of positive molds for the base, lower four bar linkage, upper four bar linkage and end effector, and flexure joints. (1) 3D models of each are produced using CAD software, and the resulting molds are fabricated using a layered wax deposition machine (3D Systems ThermoJet 8080). (2) Liquid PDMS rubber is poured into the positive molds and allowed to cure to make negative molds. (3) Cross flexure modules are fabricated separately in two halves by inserting a polyester (PET) flexural strip 100μm thick into a rubber mold and pouring two-part polyurethane (Tap Plastics Quik-Cast^{TM}) into the voids representing the rigid ends. The two halves are then stacked in such a way that the flexural strips are oriented at 90° to each other and cross at the center of the joint (Fig. 6). (4) Once cured, the flexure modules are inserted into the upper and lower four bar linkage molds, and the two molds are stacked with a separation layer between them. The separation layer has holes in the approriate places to allow

polymer to flow between the upper four bar mold and the lower mold, creating a monolithic mechanism structure. (5) The base is also fabricated using molding, and once it cures, the four bar mechanism is mated to it and RC servos are mounted and mated to the actuated links of lower four bars. The whole manipulator is then bolted to a manual vertical translation stage that is attached to the ground plane. The final assembly is shown in Fig. 7.

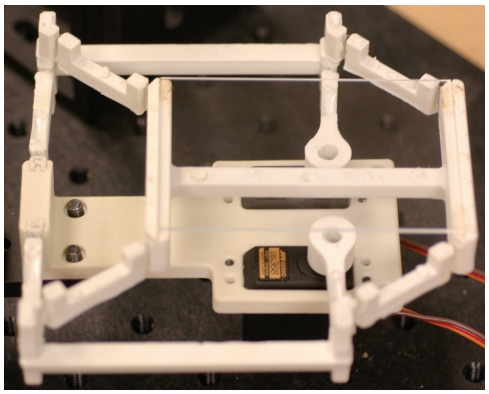

Fig. 7. Fully assembled planar balanced double four bar manipulator using compliant mechanisms

III. GRIPPER DESIGN AND FABRICATION

In previous work, it has been shown that by appropriately choosing the stiffness of the fingers in a two finger grasp, it is possible to use slip to achieve stable and robust grasping of polygonal objects without object model information [3]. Orthogonally oriented tweezer tips, or the Orthotweezers [13] [15], can take advantage of this principle to dextrously manipulate microparts 200μm on a side and 100μm tall. The gripper design we present is similarly based on the concept of orthogonally oriented fingertips.

In order to simplify and reduce the cost of the system, we again make use of rapid prototyping technologies and compliant mechanisms in the design and fabrication of the Low Cost Orthotweezers. For the reasons stated in [5] (namely a combination of cost, precision, and standardization) we have chosen digital RC servo motors as actuators for our gripper. This choice necessitates a design capable of producing a linear or approximately linear output from a rotational input.

A. Kinematic Considerations for Gripper Design

The mechanism of choice for this application given its simplicity and well understood kinematics is the four bar linkage and specifically a four bar in the crank rocker configuration. A rotational input at one joint can be transmitted into an approximately linear output (for small deflections) at another joint. And, by choosing the link lengths and the reference configuration (or neutral pose) appropriately we can generate the desired output with high resolution and accuracy.

Because the microparts we intend to manipulate with the gripper have dimensions on the order of 200μm, we would like to design for individual fingertip displacements of approximately 500μm. Using this as a design guideline and modeling the compliant linkage as a set of ideal rigid links connected with pin joints as shown in Fig. 8(a), we use the well known inverse kinematics of the four bar linkage to generate the design parameters. In our calculations, θ_3 is taken to be the input angle, and θ_1 is taken as the output. An approximation of the displacement at the tip is just given by $\delta = l_1(\theta_{10} - \theta_{11})$. Table II summarizes the design parameters for a single four bar finger linkage. For the design parameters listed, we obtain a 700μm output at the finger tip for a 10° input from the actuator. For digital servos with approximately 10 steps per degree, our design yields a resolution of 7μm per step.

B. Gripping Force Considerations

In [13] it was shown that by modeling the fingertips as linear beams, and designing them to have a tip compliance of 100 N/m sufficient grasping force (approx. 1mN) can be generated to achieve stable grasping as well as part rolling or rotation. Using 100N/m as our tip stiffness, the design discussed above is capable of generating forces in increments of 0.7 mN.

C. Gripper Fabrication

The gripper is fabricated using the same rapid prototyping process described for the manipulator. However, since the gripper linkage is essentially a 2.5D planar structure, only one mold is necessary. Polyester flexure material is inserted into the mold between the voids that represent the rigid links and then all voids are filled with liquid two-part polyurethane and the structure is allowed to cure before demolding. A small depression is molded into the end of the finger, l_1, to provide an alignment feature for the stainless steel fingertip. When the finger linkage is demolded, the stainless steel fingertip (2mm x 13.3mm x 50μm) is butted up against the alignment feature causing the tip to be oriented downward at an angle of 10°. This ensures that no part of the bottom portion of the finger link will come into contact with the end effector platform or any parts on its surface as the manipulator is moved beneath the gripper. Additionally, the fingertip is positioned to extend 5mm past the end of the rigid finger link. Using standard Eulerian elastic beam theory we calculate the fingertip compliance to be 98N/m using the following equations:

$$K = \frac{3EI}{L^3} \tag{9}$$

E is the elastic modulus of stainless steel which we take to be 195GPa and I for a standard rectangular cross-section beam with cross-section width w and height h is given by:

$$I = \frac{wh^3}{12} \tag{10}$$

Once the fingertips have been attached, the right and left finger linkages are attached to the RC servo motors by screwing self-threading plastite screws into holes in the

TABLE II

DESIGN PARAMETERS FOR A FOUR BAR FINGER LINKAGE

Parameter	Value
l_0	70mm
l_1	35mm
l_2	67mm
l_3	10mm
θ_3	135°
θ_1	90°
Transmission Ratio	8.33

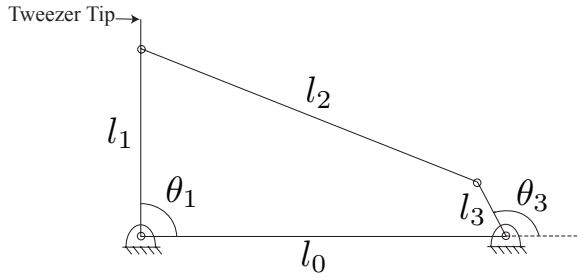

(a) Idealized model of four bar gripper

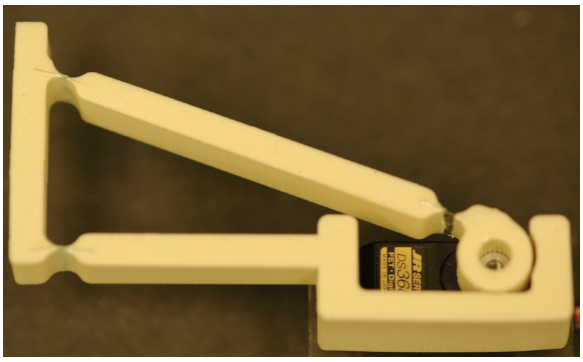

(b) Compliant four bar finger linkage with servo motor actuator attached

Fig. 8. Rigid body finger model and actual compliant finger linkage

linkage designed to align with mounting features on the servos. The servos are then bolted onto a ground plane at right angles to each other and each finger is adjusted so that the fingertips are aligned with approximately 500μm between them.

IV. VISION-BASED MANIPULATOR CALIBRATION

Because the fabrication process introduces uncertainty into the kinematics of the planar balanced double four bar mechanism, calibration is necessary to achieve precise positioning of the end effector. The classic approach to calibration attempts to fit parameters of the kinematic model to experimental data collected using some sensor(s). However, our rapid prototyping process is likely to be a large source of error in the mechanism kinematics. In fact, the errors may be large enough and may exist in enough features of the final mechanism that our idealized kinematic model in Eqns. (2 - 5), with only two independent parameters, may not fit the data accurately enough for our requirements. So, rather than attempt to introduce more parameters into the kinematic model, we have chosen to use a piecewise linear barycentric interpolation scheme over a large amount of experimental data to interpolate the kinematic functions.

A. Calibration Pattern

We begin by designing a calibration pattern for the extraction of absolute position from an image captured under a digital microscope webcam. The pattern consists of a grid of lines spaced at 2mm in the X direction and 1.5mm in the Y direction. Within each grid cell is a pattern of dots arranged in three rows of four dots. Each dot represents a bit in a 12bit binary number with the upper left bit being the least significant and the lower right bit being the most significant bit. Cells are numbered from the upper left to the lower right corner of the pattern, with upper the left starting at zero. The geometry of the grid ensures that at 20X zoom of the microscope camera at least one entire grid cell is always in the field of view. The microscope camera used comes as part of the Motic DS300 USB field microscope kit and provides 640x480 resolution, giving 6.25μm per pixel resolution at 20X zoom and 3.125μm per pixel at 40X zoom.

The calibration pattern is placed on the end effector of the manipulator and each actuated joint of the manipulator is commanded over a 90° range in increments of 1.8° (2500 positions). At each position an image is captured. The image is processed according to the algorithm shown in Fig. 9. An image before and after processing is shown in Fig. 10. The corners of the red outline are the vertices of the rectangular bounding box for the region of interest (ROI) and the green grid lines indicate the division of the ROI into dodecant sub-ROIs. The number in the upper left corner encodes the absolute position of the center of the ROI.

Results of capturing calibration data using the vision-based algorithm from Fig. 9 are shown in Fig. 11. By comparing the theoretical model depicted in Fig. 5 with the experimental calibration data from Fig. 11 we can see that the experimental data agree well with the theoretical kinematic model.

V. EXPERIMENTAL RESULTS AND SYSTEM PERFORMANCE

For operation, the camera is interfaced through USB with a PC running the Linux operating system. The controller board for the servo motors that actuate both the manipulator platform and the gripper (PicoPic, Picobotics Inc.) interfaces with the same PC using the serial protocol. The whole system is programmed in Python and makes extensive use of the free, open source computer vision library, OpenCV [1]. This is the setup that is used to collect experimental data.

A. Manipulator Performance

In characterizing the performance of the manipulator we examine two measures, namely Euclidean position error and repeatability. The position error is a measure of the difference between the commanded or expected position and the position as measured by the camera using the same method described in the previous section on calibration.

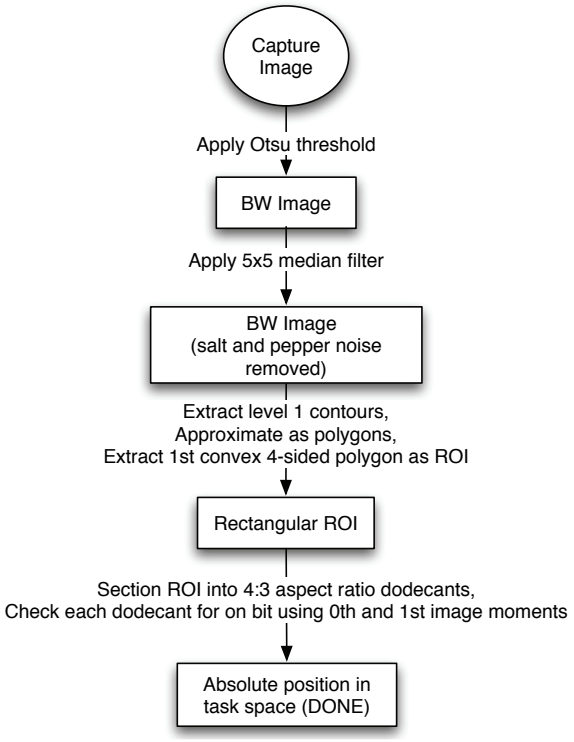

Fig. 9. Vision algorithm for extracting absolute end effector position from images of a calibration pattern

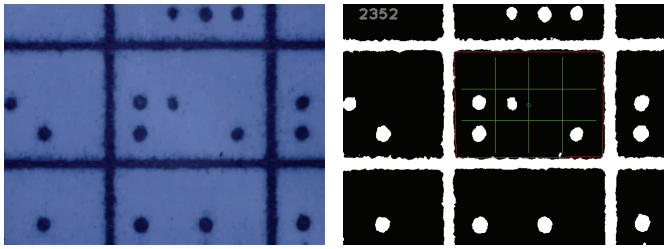

(a) Unprocessed calibration image (b) Processed calibration image with binary position data parsed

Fig. 10. Sample results of image processing algorithm for extracting position from image data used in calibration

The repeatability measures how reliably the manipulator can return to the same position many times. The positional error will contain errors due to the linear interpolation scheme as well as the effects of actuator quantization. That is, the actuators have some finite resolution (approximately 0.09°), making the manipulator incapable of reaching an arbitrary position in the workspace.

Table III summarizes the positioning accuracy/error results obtained by taking 1000 position samples at each of four different manipulator positions in the task space. The overall maximum Euclidean position error is found to be 173μm while the maximum mean positioning error is 145μm. We define positioning error as the distance of the observed position from the commanded position. However, in Table IV we see that at each of those positions the manipulator shows a mean repeatability to within 23μm with the worst overall

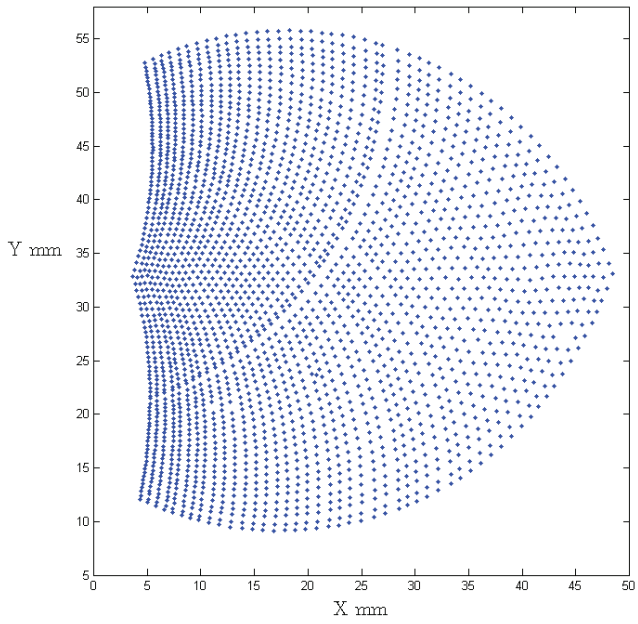

Fig. 11. Approx. 2500 experimentally sampled task space output positions resulting from uniform actuator inputs in increments of 1.8°.

TABLE III
POSITIONING ACCURACY RESULTS AT FOUR DIFFERENT WORKSPACE POSITIONS

Workspace Position (mm)	45, 25	45, 35	35, 35	35, 25
Mean Error (μm)	135	145	73	104
Std. Deviation (μm)	10	15	14	16
Min. Error (μm)	104	107	28	75
Max. Error (μm)	173	196	117	134

observed repeatability being 86 μm. We define repeatability as the distance from the mean observed position for a set of repeatedly specified actuator commands. Assuming we begin an assembly process with our parts in a known reachable position and orientation, we can use the maximum repeatability error to generate an upper bound on gripper forces since we know the equivalent spring constants of our gripper fingertips. From the results in Table IV, we find that the absolute maximum repeatability error is approximately 86μm. Multiplying this maximum displacement by finger stiffness we get an upper bound of 8.6mN on the passive gripping force.

TABLE IV
POSITIONING REPEATABILITY RESULTS AT FOUR DIFFERENT WORKSPACE POSITIONS

Workspace Position (mm)	45, 25	45, 35	35, 35	35, 25
Mean Repeatability (μm)	15	14	23	17
Std. Deviation (μm)	8	9	16	7
Min. Repeatability (μm)	3	1	3	3
Max. Repeatability (μm)	46	54	86	38

B. Gripper Performance

Fig. 12 shows a sequence of images demonstrating the ability of the gripper to grasp a 200μm square part and rotate it by 45°. All gripping operations were performed open loop. A human operator commanded the manipulator to position the part within the gripping envelope while visually monitoring the process using the microscope camera.

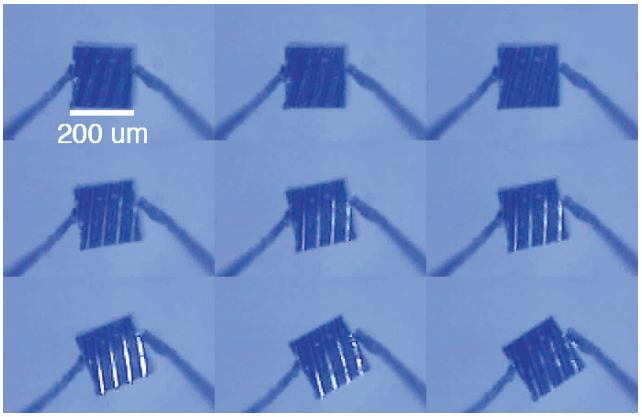

Fig. 12. Open loop rotation of a 200μm square silicon block by 45° using the Low Cost Orthotweezers

VI. CONCLUSIONS AND FUTURE WORK

A. Conclusions

We have presented the first iteration of a rapidly prototyped microassembly/micromanipulation cell that is fabricated inexpensively using rapid prototyping processes, commodity actuators, electronics and hardware, and free, open source software having an overall cost (excluding the PC used for programming and data capture) less than $500. Our system provides 3 degrees of freedom (XY translation and θ rotation), and we have demonstrated that our manipulator design is capable of positioning microparts with sufficient repeatability to allow for grasping. We have also demonstrated that the compliant four bar linkage-based gripper design is capable of both grasping and rotating 200μm x 200μm x 100μm microparts. Lastly, we characterized the noise in the system and from that developed an upper bound on the grasping forces for a worst case grasp.

B. Future Work

Future work will include integrating an actuated Z axis for positioning, again using compliant mechanisms. The introduction of a third axis will enable full automation of the manipulation and assembly process. As well, we aim to more fully integrate vision-based feedback. We would like to develop robust algorithms for part picking and placement, and we also hope to reduce true position error by using visual servoing based on object recognition or image cross-correlation.

VII. ACKNOWLEDGEMENTS

This work was supported under NSF DMI Grant No. 0423153. The authors thank Erik Steltz and Minerva Pillai for their help, insight, and thought-provoking conversations.

REFERENCES

[1] [Online]. Available: http://opencvlibrary.sourceforge.net
[2] Y. H. Anis, J. K. Mills, and W. L. Cleghorn, "Vision-based measurement of microassembly forces," *Journal of Micromechanics and Microengineering*, vol. 16, no. 8, pp. 1639–1652, 2006. [Online]. Available: http://stacks.iop.org/0960-1317/16/1639
[3] R. Fearing, "Simplified grasping and manipulation with dextrous robot hands," *IEEE J. Robotics and Automation*, vol. 2, no. 4, pp. 188–195, Dec. 1986.
[4] P. Ferreira, J. Dong, D. Mukhopadhyay, Q. Yao, and E. Pengwang, "Study of low degree-of-freedom parallel kinematics for multi scale manufacturing applications," in *Design, Service, and Manufacturing Grantees and Research Conference*. St. Louis, MO: NSF, July 2006.
[5] A. M. Hoover, R. E. Groff, S. Avadhanula, and R. S. Fearing, "A rapidly prototyped 2-axis positioning stage for microassembly using compliant mechanisms," in *International Conference on Robotics and Automation*. IEEE, 2006.
[6] M. Horie, T. Uchida, and D. Kamiya, "Development of miniature pantograph mechanisms with large-deflective hinges for new surface mount systems," in *Proc SPIE Int Soc Opt Eng*, vol. 4019, 2000, pp. 546–555.
[7] L. L. Howell, *Compliant mechanisms*. John Wiley & Sons, 2001.
[8] R. Merz, F. Prinz, K. Ramaswami, M. Terk, and L. Weiss, "Shape deposition manufacturing," in *Solid Freeform Fabrication Symposium*. University of Texas at Austin, August 1994.
[9] R. M. Murray, S. S. Sastry, and L. Zexiang, *A Mathematical Introduction to Robotic Manipulation*. Boca Raton, FL, USA: CRC Press, Inc., 1994.
[10] A. Neild, S. Oberti, F. Beyeler, J. Dual, and B. J. Nelson, "A micro-particle positioning technique combining an ultrasonic manipulator and a microgripper," *Journal of Micromechanics and Microengineering*, vol. 16, no. 8, pp. 1562–1570, 2006. [Online]. Available: http://stacks.iop.org/0960-1317/16/1562
[11] C. Pawashe and M. Sitti, "Two-dimensional vision-based autonomous microparticle manipulation using a nanoprobe," *J. of Micromechatronics*, vol. 3, no. 3-4, pp. 285–306, 2006.
[12] Y. Shen, N. Xi, B. Song, J. Wen, and C. A. Pomeroy, "Networked human/robot cooperative environment for tele-assembly of mems devices," *J. of Micromechatronics*, vol. 3, no. 3-4, pp. 239–266, 2006.
[13] E. Shimada, R. Wood, J. Yan, J. Thompson, and R. S. Fearing, "Prototyping millirobots using dextrous microassembly and folding," in *International Mechanical Engineering Conference and Expo*, vol. DSC - Vol 59-2. Orlando, FL: ASME, Nov. 2000, pp. 933–940.
[14] D. Stewart, "A platform with six degrees of freedom," in *Institution of Mechanical Engineers*, vol. 180, 1965, pp. 371–378.
[15] J. Thompson and R. S. Fearing, "Automating microassembly with ortho-tweezers and force sensing," in *IROS*. IEEE, 2001.
[16] B. P. Trease, Y. Moon, and S. Kota, "Design of large displacement compliant joints," *Journal of Mechanical Design*, vol. 127, no. 4, pp. 788–798, July 2005.
[17] W. Weinstein, "Flexure-pivot bearings part 2," *Machine Design*, pp. 136–145, July 1965.
[18] R. Wierzbicki, K. Houston, H. Heerlein, W. Barth, T. Debski, A. Eisinberg, A. Menciassi, M. Carrozza, and P. Dario, "Design and fabrication of an electrostatically driven microgripper for blood vessel manipulation," *Microelectronic Engineering*, vol. 83, pp. 1651–1654, 2005.